Author/s:
Wang, Z;Cortez-Jugo, C;Yang, Y;Chen, J;Wang, T;De Rose, R;Cui, J;Caruso, F

Title:
A Metal–Phenolic Network-Enabled Nanoadjuvant to Modulate Immune Responses

Date:
2024-10-17

Citation:
Wang, Z., Cortez-Jugo, C., Yang, Y., Chen, J., Wang, T., De Rose, R., Cui, J. & Caruso, F. (2024). A Metal–Phenolic Network-Enabled Nanoadjuvant to Modulate Immune Responses. Small, 20 (42), https://doi.org/10.1002/smll.202401776.

Persistent Link:
https://hdl.handle.net/11343/350331

RESEARCH ARTICLE

NANO · MICRO small
www.small-journal.com

A Metal–Phenolic Network-Enabled Nanoadjuvant to Modulate Immune Responses

Zhaoran Wang, Christina Cortez-Jugo, Yang Yang, Jingqu Chen, Tianzheng Wang, Robert De Rose, Jiwei Cui, and Frank Caruso**

The presence of hierarchical suppressive pathways in the immune system combined with poor delivery efficiencies of adjuvants and antigens to antigen-presenting cells are major challenges in developing advanced vaccines. The present study reports a nanoadjuvant constructed using aluminosilicate nanoparticles (as particle templates), incorporating cytosine–phosphate–guanosine (CpG) oligonucleotides and small-interfering RNA (siRNA) to counteract immune suppression in antigen-presenting cells. Furthermore, the application of a metal–phenolic network (MPN) coating, which can endow the nanoparticles with protective and bioadhesive properties, is assessed with regard to the stability and immune function of the resulting nanoadjuvant in vitro and in vivo. Combining the adjuvanticity of aluminum and CpG with RNA interference and MPN coating results in a nanoadjuvant that exhibits greater accumulation in lymph nodes and elicits improved maturation of dendritic cells in comparison to a formulation without siRNA or MPN, and with no observable organ toxicity. The incorporation of a model antigen, ovalbumin, within the MPN coating demonstrates the capacity of MPNs to load functional biomolecules as well as the ability of the nanoadjuvant to trigger enhanced antigen-specific responses. The present template-assisted fabrication strategy for engineering nanoadjuvants holds promise in the design of delivery systems for disease prevention, as well as therapeutics.

1. Introduction

Vaccines are actively being pursued for the prevention of infectious diseases and the treatment of cancer. In vaccine formulations, adjuvants play an indispensable role in triggering strong and sustainable immune responses, encompassing both innate and adaptive immunity.[1] Adjuvants work with antigens to induce the secretion of pro-inflammatory factors from antigen-presenting cells (APCs) and recruit cytotoxic T lymphocytes (CTLs) to destroy foreign pathogens such as bacteria and viruses, as well as tumor cells.[2] Various adjuvants with different mechanisms, including ligands of Toll-like receptors (TLRs) such as cytosine–phosphate–guanosine (CpG),[3] aluminum salts,[4] agonists of the cyclic GMP–AMP synthase (cGAS)–stimulator of interferon genes (STING) pathway,[5] and cytokines,[6] have been widely reported. Nevertheless, the complex immune system creates a barrier to efficient and effective adjuvant performance. A challenge is achieving effective and efficient delivery of adjuvants to secondary lymphoid organs such as lymph nodes (LNs). Most adjuvants are small molecules or short nucleic acids that are susceptible to rapid clearance and/or degradation during systemic circulation. As a result, next-generation adjuvants being developed include carriers, for example, nanoparticles, to overcome physiological barriers in vivo, prevent adjuvant degradation, and ultimately influence the immune response in APCs such as dendritic cells (DCs).[7] DCs, in particular, associate directly with nanomaterials and play a central role in the immune system by bridging immune responses. Thus, engineering nanoparticles to target and regulate DCs can effectively enhance innate and adaptive immunity. Recent advancements have seen the emergence of polymer-based[8] and lipid-based[9] carriers as major vehicles in delivering immunostimulant agents. However, these carriers can present challenges in formulation uniformity, cold-chain storage, and safety, including hypersensitivity reactions.[10]

In addition to delivery challenges, the immune response can be compromised due to suppressive pathways within the immune microenvironment. Apart from the widely studied

Z. Wang, C. Cortez-Jugo, J. Chen, T. Wang, R. De Rose, F. Caruso
Department of Chemical Engineering
The University of Melbourne
Parkville, Victoria 3010, Australia
E-mail: fcaruso@unimelb.edu.au

Y. Yang, J. Cui
Key Laboratory of Colloid and Interface Chemistry of the Ministry of Education, School of Chemistry and Chemical Engineering
Shandong University
Jinan, Shandong 250100, China
E-mail: jwcui@sdu.edu.cn

The ORCID identification number(s) for the author(s) of this article can be found under https://doi.org/10.1002/smll.202401776

DOI: 10.1002/smll.202401776

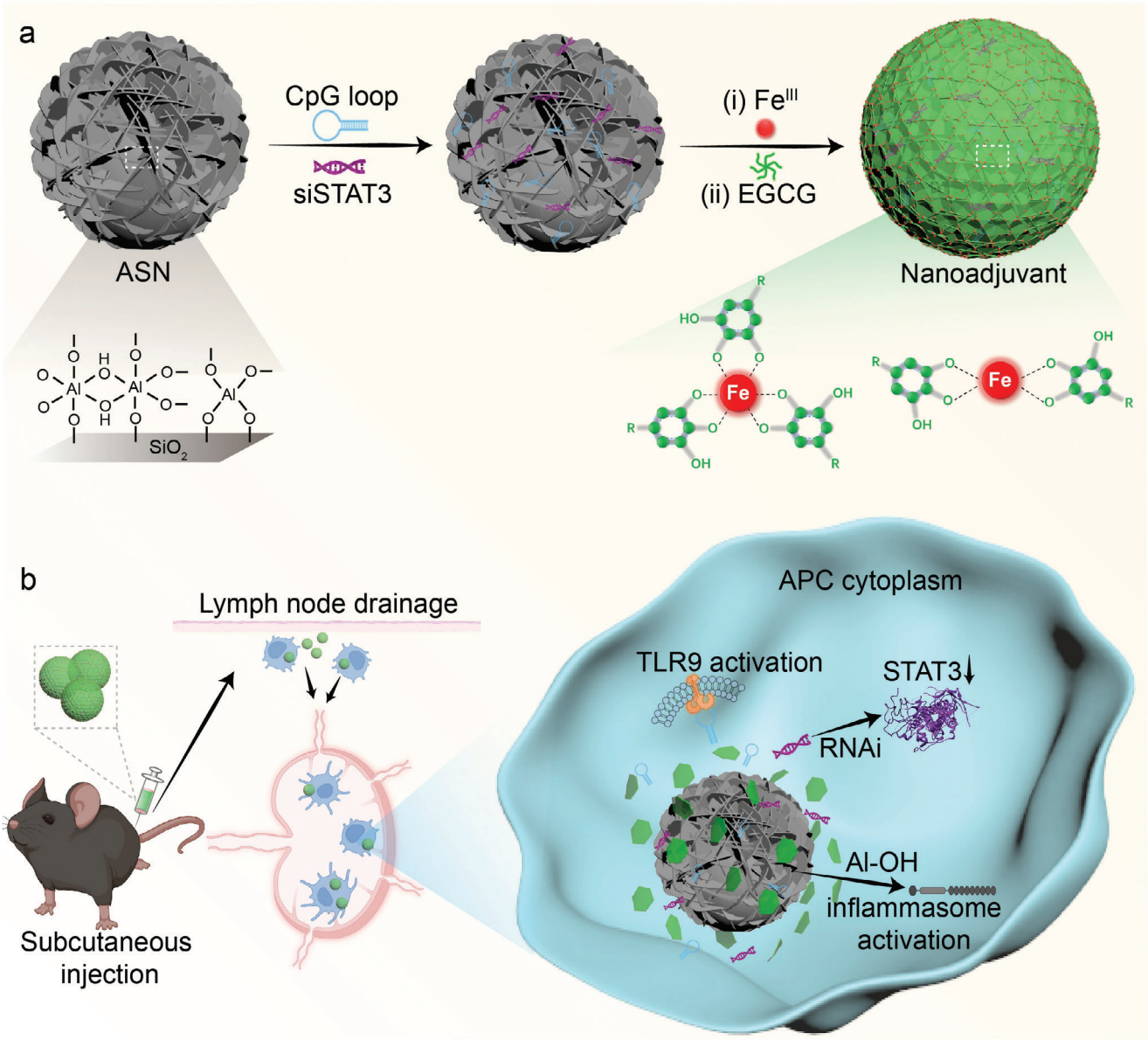

Scheme 1. Assembly and intracellular function of the multicomponent nanoadjuvant. a) Illustration of the preparation of the ASN nanoadjuvant loaded with anti-STAT3 siRNA (siSTAT3) and CpG and subsequently coated with a metal–phenolic (Fe^{III}–EGCG) film. b) Designed multifunctionality of the nanoadjuvant after drainage into LNs post subcutaneous injection and internalization by DCs including TLR recognition, inflammasome activation, and target gene (STAT3) knockdown for enhanced adjuvanticity.

immune checkpoints including programmed cell death protein 1 (PD-1) and cytotoxic T lymphocyte-associated protein 4 (CTLA-4),[11] some intracellular signaling pathways, such as the signal transducer and activator of transcription 3 (STAT3) signaling pathway, can negatively impact the function of TLR agonists in APCs, leading to a suppressed immune response.[12] To address this issue, RNA interference has emerged as a powerful approach to modulating the immune response by knocking down the expression of immunosuppressive proteins.[13] In this strategy, small-interfering RNA (siRNA) can be combined with adjuvants (e.g., CpG) in a single formulation to alleviate immune suppression and enhance immunostimulation.

Here, we report the synthesis of a nanoadjuvant based on aluminosilicate nanoparticles (ASNs) that co-delivers CpG oligonucleotides for TLR9 stimulation and anti-STAT3 siRNA (siSTAT3) to regulate responses in APCs (**Scheme 1**). Mesoporous silica nanoparticles (MSNs) have been investigated as versatile drug carriers owing to their large specific surface area, easy-to-control size distribution, and good stability in biological milieus.[14] Upon chemical reaction with aluminum salt, MSNs are converted to ASNs—aluminum-infused positively charged silica derivatives that serve as both an adjuvant and a delivery vehicle for immunogenetic cargos. The ASNs are an improved formulation of the commercially available Alum adjuvant and

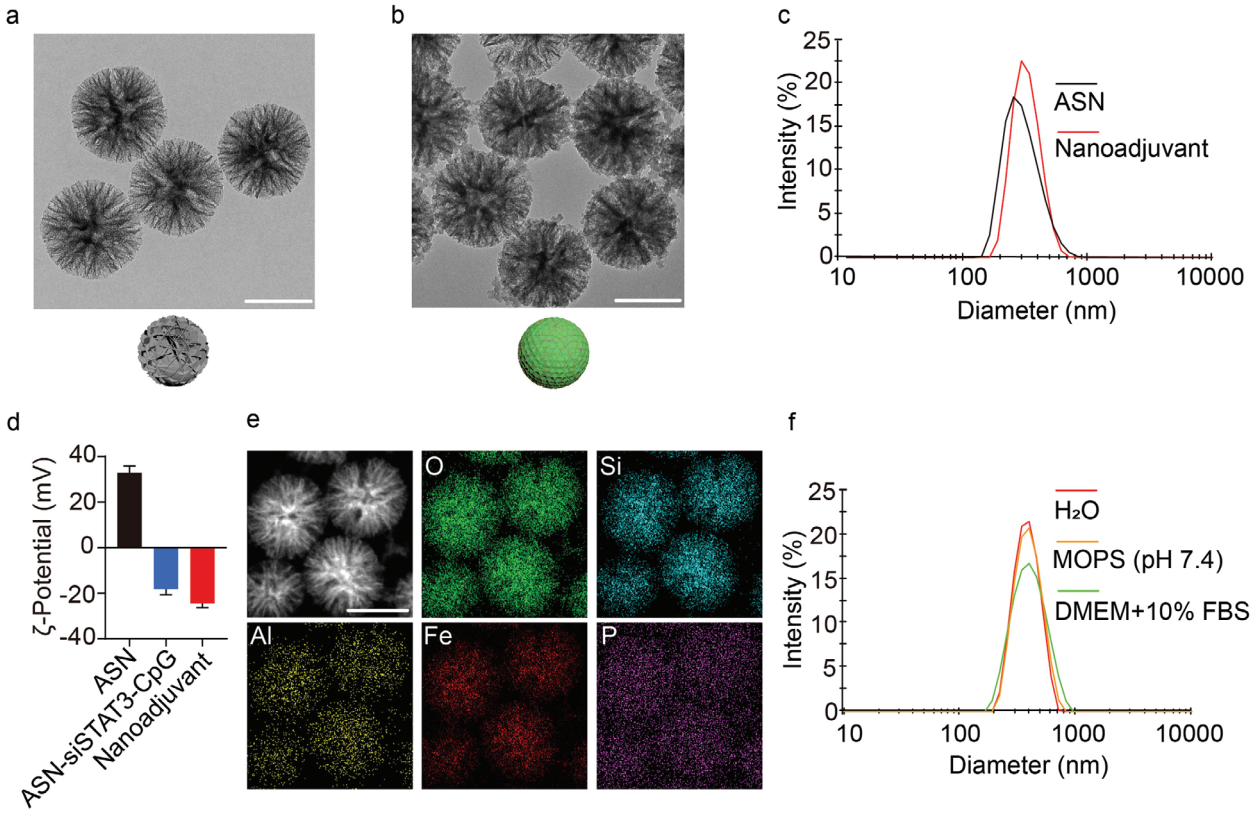

Figure 1. Characterization of the Nanoadjuvant. Representative TEM images of a) bare ASNs and b) the Nanoadjuvant. Scale bars: 200 nm. c) Hydrodynamic diameters of bare ASNs and the Nanoadjuvant measured in water by dynamic light scattering. d) ζ-Potential of ASNs before and after loading with siSTAT3 and CpG and post-MPN coating. Data are shown as the average mean ± standard error of the mean, from $n = 3$ particle synthesis replicates. e) EDX mapping of the Nanoadjuvant showing the presence of O, Si, Al, Fe, and P. Scale bar: 200 nm. f) Hydrodynamic diameters of the Nanoadjuvant in water (H_2O), MOPS buffer, and cell culture medium (Dulbecco's Modified Eagle Medium (DMEM)+10% fetal bovine serum (FBS)), as measured by dynamic light scattering.

induce enhanced cellular immunity through inflammasome activation and reduced neurotoxicity.[15] The prepared ASNs are then coated with metal–phenolic networks (MPNs) (Scheme 1), which are organic–inorganic hybrid materials composed of natural polyphenols coordinated with metal ions.[16] Our previous studies have shown the rapid and simple assembly of MPNs into diverse functional platforms, including nanoparticles and thin film coatings.[17] Using a library of phenolic ligands and metal ions, MPNs can be engineered to display various surface properties particularly when deposited on particle substrates via hydrogen bonding and hydrophobic interactions.[18] The interactions of polyphenols with functional polymers, chemotherapeutic drugs, proteins, as well as nucleic acids have been exploited in the delivery of active cargo.[19] Inspired by these properties, we hypothesize that MPNs as a coating layer would benefit cellular uptake and LN accumulation of immunogenic nanoparticles. Accordingly, MPNs consisting of Fe^{III} and epigallocatechin gallate (Fe^{III}–EGCG) are applied as a protective layer on the surface of the ASNs. The Fe^{III}–EGCG MPN coating improved cell association and accumulation in draining lymph nodes (dLNs), ensuring efficient gene knockdown function of siSTAT3 and adjuvanticity of CpG in APCs. Moreover, the MPN layer enabled post-loading of the nanoadjuvant with a model antigen, that is, ovalbumin (OVA), displaying the vaccination potential of our multifunctional nanoparticle platform. The merits of our nanoadjuvant summarized above are expected to contribute to next-generation vaccine development based on natural and biocompatible formulations.

2. Results and Discussion

2.1. Assembly and Characterization of the Nanoadjuvant

ASNs were synthesized via chemical surface modification of MSNs according to a previously reported protocol.[15] Briefly, aluminum salt solution was slowly mixed with MSNs dispersed in sodium acetate buffer and incubated for 3 h in an oil bath at 60 °C to allow the hydrolyzed aluminum species to react with silanol groups on the surface of MSNs. Uniformly dispersed ASNs with diameters of 270 ± 5 nm (**Figure 1a**) were obtained, as determined by transmission electron microscopy (TEM). siSTAT3 and CpG (sequences listed in Table S1, Supporting Information) were loaded on the porous surface of ASNs via electrostatic interaction, as confirmed by the change in ζ-potential from 33 to −18 mV after loading (Figure 1d). The encapsulation capacity of siSTAT3 and CpG within the ASNs was examined by agarose gel electrophoresis, which enables the detection of free or nonloaded nucleic acids. As determined from the

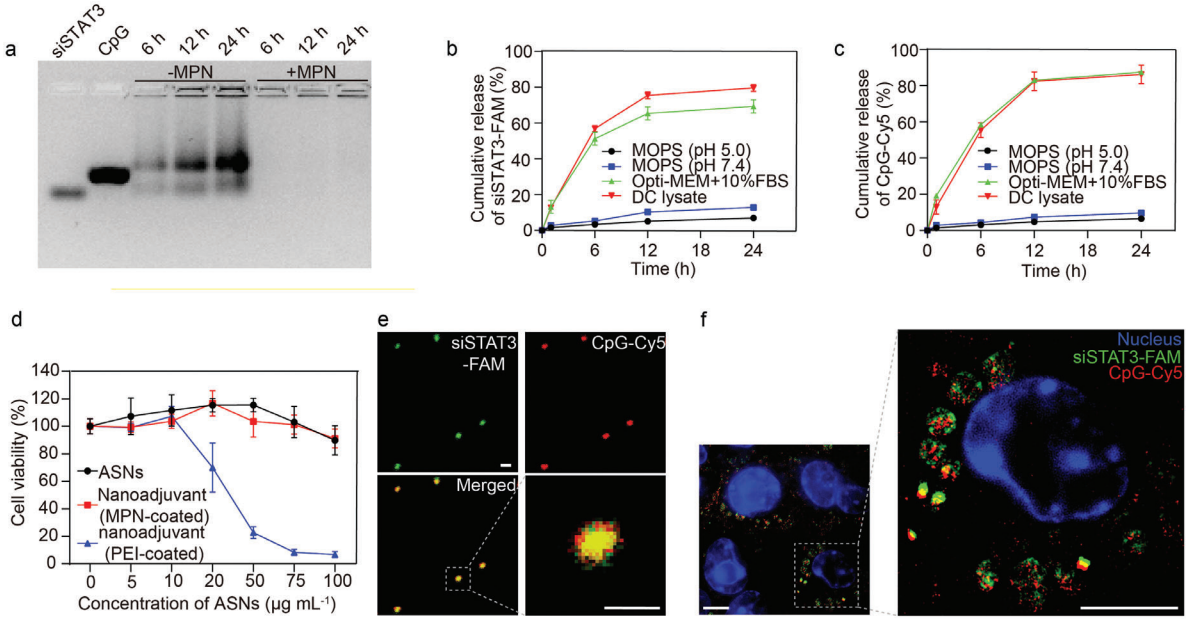

Figure 2. Stability, release profiles, and cellular uptake of the Nanoadjuvant. a) Agarose gel electrophoresis image showing unbound siSTAT3 and CpG from suspensions of nanoadjuvants without (−MPN) and with (+MPN) an MPN coating after 6, 12, and 24 h incubation in MOPS (pH 7.4) at room temperature. Cumulative release of b) siSTAT3 and c) CpG from the Nanoadjuvant in MOPS (pH 5.0 and pH 7.4), cell culture medium, and lysate of DCs over 24 h at 37 °C. Data represents mean ± standard deviation (s.d.) ($n = 3$). d) Viability of RAW264.7 cells after incubation with ASNs, the Nanoadjuvant (with an MPN coating), or nanoadjuvant with a PEI coating for 24 h at 37 °C. Data are shown as mean ± s.d. ($n = 5$). e) Fluorescence images showing the colocalization of siSTAT3-FAM and CpG-Cy5 on the Nanoadjuvant prior to intracellular delivery. Scale bars: 500 nm. f) SIM images of distribution of siSTAT3 (green) and CpG (red) after internalization of the Nanoadjuvant by RAW264.7 cells after 4 h. Scale bars: 5 μm.

gel electrophoresis data in Figure S1 (Supporting Information), 20 μg of ASNs was sufficient to encapsulate 1 μg of siSTAT3 and 2 μg CpG. Hence, weight ratios of w_{ASN}:$w_{siSTAT3}$ = 20:1 and w_{ASN}:w_{CpG} = 10:1 were used for loading in subsequent experiments. An MPN layer of Fe^{III}–EGCG was then deposited after nucleic acid loading, which reduced the ζ-potential further to −24 mV (Figure 1d). The proportion of each component in the nanoadjuvant is summarized in Table S2 (Supporting Information). As determined from TEM analysis in Figure 1b, the final particles (siSTAT3- and CpG-loaded ASNs and coated with MPNs), referred to thereafter as Nanoadjuvant, were only slightly larger (279 ± 5 nm) than the bare ASNs owing to nucleic acid loading and MPN coating. This minor change in size was also observed via dynamic light scattering analysis (Figure 1c). Energy-dispersive X-ray (EDX) mapping confirmed the presence of the individual components within the Nanoadjuvant, that is, Al and Si in ASNs, P in nucleic acid, and Fe in the MPN layer (Figure 1e). The Nanoadjuvant was stable and well dispersed in buffer solution (3-(N-morpholino) propanesulfonic acid, MOPS, pH 7.4) and cell culture media (containing 10% fetal bovine serum) with hydrodynamic diameters (≈370 nm) similar to those determined in Milli-Q water (Figure 1f).

2.2. MPN-Assisted Stabilization of the Nanoadjuvant and Intracellular Trafficking

The degradability of the Nanoadjuvant was assessed via agarose gel electrophoresis. Cargo (siSTAT3+CpG)-loaded ASNs with or without an MPN coating were incubated in MOPS buffer (pH 7.4) at room temperature and nucleic acid release in the supernatant was assessed. Negligible release of nucleic acid from the Nanoadjuvant (coated with MPNs) was observed over a 24 h period, indicating the protective capacity of the Fe^{III}–EGCG MPN layer under physiological pH condition (**Figure 2**a). Moreover, the MPN-coated particles were retained in the wells without the release of siSTAT3 or CpG upon immediate loading of the Nanoadjuvant after assembly, (Figure S2, Supporting Information). The release conditions of carboxyfluorescein (FAM)-labeled siSTAT3 and cyanine 5 (Cy5)-labeled CpG from the Nanoadjuvant were then investigated in different milieus at 37 °C (Figure 2b,c; Figure S3, Supporting Information). Only ≈10% of total siSTAT3-FAM and CpG-Cy5 were released in MOPS after 24 h, regardless of pH. Although MPN stability has been reported to be dependent on pH,[20] complete degradation of the MPN coating was not observed when applied to highly positively charged ASNs. ζ-Potential analysis of the ASNs showed a gradual change to positive charge at low pH (Figure S4, Supporting Information), which facilitates the strong binding of nucleic acids and consequently slows their release, particularly at lower pH. In contrast, siSTAT3 and CpG were released from the Nanoadjuvant when incubated in DC lysate and cell culture medium containing 10% serum, with >70% released within 24 h. We speculate that proteins present in cell culture medium and cell lysate compete with siSTAT3 and CpG for binding on ASNs and MPNs, leading to the displacement of siSTAT3 and CpG.

To improve reproducibility, reporting, and re-analysis, this study conforms to the Minimum Information Reporting in

Bio–Nano Experimental Literature standard,[21] and a companion checklist is provided in the Supporting Information. The cellular fate of the Nanoadjuvant was evaluated in a macrophage cell line, RAW264.7, as a model APC. The viability of RAW264.7 cells after treatment for 24 h with ASNs, Nanoadjuvant (with an MPN coating), or nanoadjuvant with a polyethylenimine (PEI) coating was examined using a cell counting kit-8 viability assay (Figure 2d). With increasing ASN concentration, cells treated with the Nanoadjuvant maintained higher cell proliferation (>85% cell viability after treatment with up to 100 μg mL^{-1} ASNs) compared to nanoadjuvant coated with PEI (<10% cell viability), highlighting the low cytotoxicity of MPNs as a coating relative to PEI. To ensure optimal cellular function, an ASN concentration of 50 μg mL^{-1} was chosen in further cellular experiments. Intracellular co-delivery of siSTAT3 and CpG by the Nanoadjuvant in RAW264.7 cells was investigated by structured illumination microscopy (SIM). As observed from Figure 2e, the two payloads colocalized uniformly within the Nanoadjuvant. At 4 h post incubation with cells, the cells displayed strong cytosolic fluorescence signals owing to siSTAT3-FAM and CpG-Cy5 (Figure 2f; Figure S5, Supporting Information). The overlapping signals (yellow) demonstrated colocalization of the two nucleic acids within the cells, whereas the scattered fluorescent events indicated the release of siSTAT3 and CpG from the nanoparticles. The cell association of the nanoadjuvants was also tested in a mouse dendritic cell line (DC1940). As shown in the confocal laser scanning microscopy (CLSM) images in Figure S6 (Supporting Information), after incubating cells with the MPN-coated ASNs, more fluorescently labeled siSTAT3 was present after 24 h, indicating that the MPN coating could help improve cell association and cargo delivery. This improvement could be ascribed to the bioadhesive property of polyphenols in the MPN, which facilitates strong binding with diverse cargos[22] and the cell membrane.[23]

2.3. Gene Silencing

Gene regulation by the nanoadjuvants at the cellular level was first analyzed on model HeLa–enhanced green fluorescent protein (EGFP) cells by flow cytometry (**Figure 3a**) and fluorescence microscopy (Figure S7, Supporting Information). Transfection of siRNA against EGFP (siEGFP) by Lipofectamine RNAiMAX, a potent transfection agent used as a positive control, had the greatest silencing effect on EGFP expression (56% knockdown), as expected, followed by the ASN-siEGFP particles coated with MPNs. Without an MPN coating, the siEGFP transfection efficiency decreased by ≈15%, possibly due to fewer siRNA being encapsulated and delivered intracellularly, as supported by the agarose gel (Figure 2a) and cell imaging (Figure S6, Supporting Information) data. To evaluate the gene modulation ability of the nanoadjuvants in immune cells, western blot analysis was performed to detect STAT3 protein from cell lysates of DC1940 treated with siSTAT3-containing nanoparticles, as well as control particles. As depicted in Figure 3b and Table S3 (Supporting Information), ASN-siSTAT3 assembled with an MPN coating displayed comparable down-regulation of STAT3 with the RNAiMAX-transfected group and better efficacy than nanoparticles without an MPN coating.

2.4. Nanoadjuvant-Induced Enhancement of APC Activation In Vitro

Immunological assays were conducted to evaluate the activation of APCs in response to the Nanoadjuvant. Activation of APCs is the first and significant step in generating immune responses against pathogens. Primary bone marrow-derived dendritic cells (BMDCs) obtained from C57BL/6 mice were cultured and treated with different nanoadjuvant groups. The maturation level of DCs was assessed by detecting co-stimulatory factors CD80/CD86, and major histocompatibility complex class II (MHC II), which is responsible for antigen presentation, using antibody staining in combination with flow cytometry analysis (Figure 3c,d; Figure S8, Supporting Information). Based on the proportions of $CD11c^+CD80^+$, $CD11c^+CD86^+$, and $CD11c^+$MHC II^+ DCs, bare ASNs had inherent adjuvanticity, and the immunity was boosted when siSTAT3 and CpG were loaded (Nanoadjuvant). As for the adjuvant groups lacking either siSTAT3 or an MPN coating, the percentage of activation was lower than that of the Nanoadjuvant. This finding indicated that siSTAT3 could inhibit the immunosuppressive pathway in these cells to elicit higher adjuvanticity, whereas the MPN coating could protect the cargos during delivery and improve cellular uptake by DCs. Nanoadjuvant-treated BMDCs were also assessed for cytokine excretion, including mouse interleukin-12 p40 (IL-12p40) (Figure 3e) and tumor necrosis factor-α (TNF-α) (Figure 3f). The production of these pro-inflammatory factors mainly follows TLR activation during DC maturation, which is a key mechanism for coordinating and strengthening immune responses. We observed a marked increase of cytokine level with the Nanoadjuvant group compared to other treatments. Thus, the combination of siSTAT3 and an MPN coating enhanced the maturation of APCs in vitro by promoting CpG-mediated adjuvanticity. The immune responses (i.e., activation and cytokine excretion) may also be partly attributed to the activation of inflammasome, which can be triggered by aluminum species in APCs, resulting in the production of reactive oxygen species (ROS).[24] To quantify the level of ROS, BMDCs were treated with different adjuvant groups for 24 h. Cell-permeable 2′,7′-dichlorodihydrofluorescein diacetate was then added to the cells as a fluorescent ROS indicator that was quantified by flow cytometry (Figure S9, Supporting Information). Among the different treatment groups examined, the Nanoadjuvant-treated BMDCs triggered the most ROS production, likely resulting from the alleviation of immune suppression by siSTAT3.

2.5. In Vivo Distribution and Adjuvanticity of the Nanoadjuvant

We then investigated the immunological activity of the Nanoadjuvant in vivo. APCs in dLNs are major participants in immunity induced by nanoparticles. They can sequester and transport nanoparticles, particularly those that are >100 nm in diameter, from the tissue to dLNs, which would be the likely mechanism for LN accumulation of our ≈280 nm nanoadjuvant.[7a,25] LN accumulation was assessed by subcutaneous injection of MPN-coated ASNs containing siSTAT3-Cy5.5 at the tail base of C57BL/6 mice. After 24 h, mice were sacrificed and major organs along with two dLNs, namely inguinal and axillary LNs, were harvested for

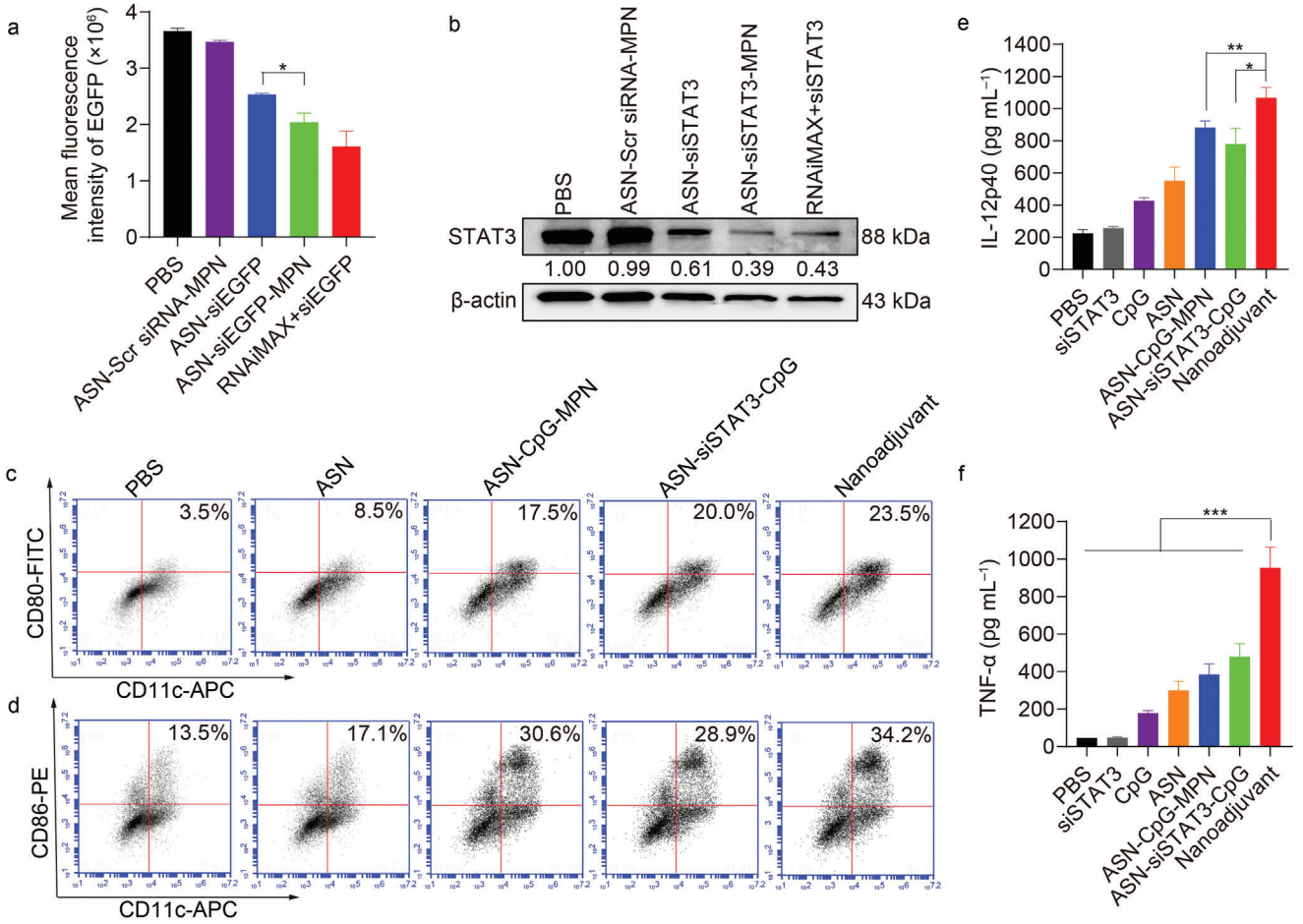

Figure 3. Gene silencing effects and immunological function at the cellular level. a) Mean fluorescence intensity of HeLa–EGFP cells after EGFP gene silencing by ASN loaded with siRNA (scrambled (Scr) siRNA or siEGFP) with or without an MPN coating and RNAiMAX+siEGFP. Data are presented as mean ± s.d. ($n = 3$). PBS, phosphate-buffered saline. b) Protein level of STAT3 in DCs regulated by MPN-coated ASN-siSTAT3 and other siSTAT3-containing formulations. Normalized values of the STAT3/β-actin band intensities are indicated. Representative flow cytometry analyses of in vitro c) CD80 and d) CD86 expression on BMDCs after treatment with ASNs, nanoadjuvant without an MPN coating, nanoadjuvant with no siRNA, or the Nanoadjuvant. FITC, fluorescein isothiocyanate; PE, phycoerythrin; APC, allophycocyanin. Secretion of cytokines e) IL-12p40 and f) TNF-α by BMDCs after treatment with the Nanoadjuvant and control groups. Data are presented as mean ± s.d. ($n = 3$). Statistical analysis was conducted via one-way analysis of variance (ANOVA) with Tukey's multiple comparison test. $^{*}p < 0.05$, $^{**}p < 0.01$, $^{***}p < 0.001$.

fluorescence imaging. Compared to the formulation without the MPN coating, the MPN-coated group displayed stronger (1.6-fold in inguinal LNs and 1.5-fold in axillary LNs) Cy5.5 signal (**Figure 4a**; Figure S10, Supporting Information). The improved accumulation of siSTAT3-Cy5.5 fluorescence signal might be ascribed to the protective effect of nucleic acids by the MPN coating during delivery as well as the strong bioadhesion of polyphenols, slowing the degradation process and potentially increasing their retention in the dLNs. The MPN-coated formulation also displayed apparent fluorescence intensity in dLNs when imaged alongside other major organs (Figure 4b; Figure S10, Supporting Information), suggesting effective in vivo delivery to secondary lymphoid organs. The retention of siSTAT3 delivered by MPN-coated nanoparticles in the dLNs was more enhanced after 48 h, that is, 2.4-fold in inguinal LNs and 1.6-fold in axillary LNs compared with nanoparticle control without an MPN coating (Figure S11, Supporting Information). Frozen sections of mice inguinal LNs at 48 h post injection (Figure 4c) were prepared. CLSM analysis indicated that in the presence of an MPN coating, the intensity of siSTAT3-Cy5.5 in LNs was higher, due to improved accumulation, than that in the absence of an MPN coating. The adhesive property of MPNs likely promotes nanoadjuvant association with APCs for prolonged drainage to LNs. The co-delivery of siSTAT3 and CpG was also examined in the frozen LN sections to verify that the Nanoadjuvant remained intact in the LNs 4 h post injection (Figure S12, Supporting Information); the fluorescence signals from siSTAT3-FAM and CpG-Cy5 overlapped, thus implying that both cargos were present, potentially within the intact Nanoadjuvant particles.

On the basis of the accumulation findings of the nanoadjuvant in the dLNs, we studied the in vivo activation of APCs. C57BL/6 mice were administered subcutaneously at the tail base with the same adjuvant groups that were assessed in vitro in BMDCs. After monitoring for 7 days, inguinal LNs were harvested and digested to obtain a single cell suspension for flow cytometry analysis. Cell mixtures were stained with antibodies against

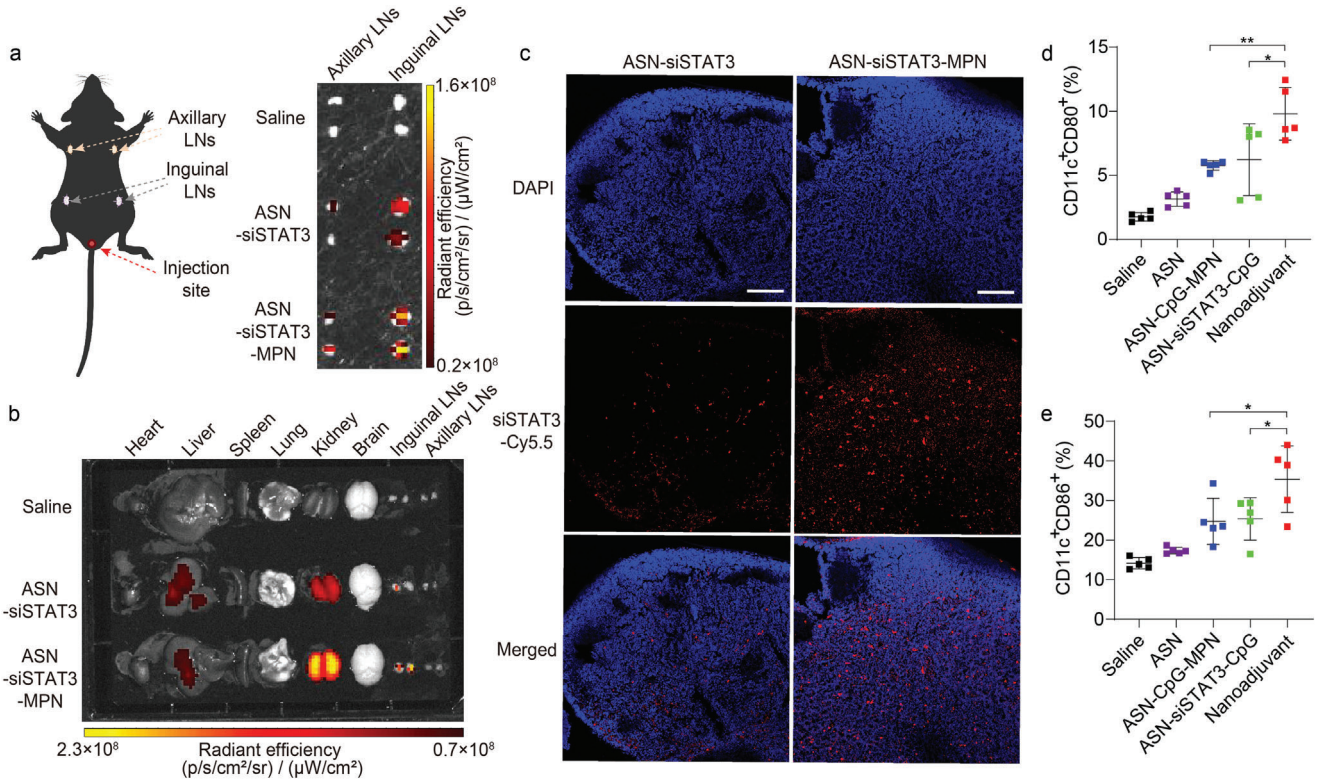

Figure 4. In vivo biodistribution and adjuvanticity. a) Fluorescence images of axillary and inguinal LNs harvested from C57BL/6 mice 24 h after subcutaneous tail base injection with saline and ASN-siSTAT3 with or without an MPN coating. b) Fluorescence images of LNs along with major organs from mice subjected to saline and ASN-siSTAT3 with or without MPN coating treatments. c) CLSM images of frozen sections of mice inguinal LNs 48 h after subcutaneous injection with ASN-siSTAT3-Cy5.5 with or without an MPN coating. Scale bars: 100 μm. Nuclei were labeled with 4′,6-diamidino-2-phenylindole (DAPI) (blue), and the siRNA within the particles was labeled with Cy5.5 (red). Level of d) CD80 and e) CD86 expression on lymphatic DCs induced by the Nanoadjuvant and other control formulations in vivo. Data represent mean ± s.d. ($n = 5$). Statistical analysis was performed via one-way ANOVA with Tukey's multiple comparison test. $^{*}p < 0.05$, $^{**}p < 0.01$.

CD11c, CD80, and CD86 for matured DC selection. We observed a marked increase in CD80 and CD86 expression (Figure 4d,e; Figure S13, Supporting Information) in the Nanoadjuvant group compared to counterpart nanoparticle formulations without siSTAT3 or an MPN coating, which is consistent with our in vitro findings. This suggests that the co-delivery of siSTAT3 and CpG by ASNs, along with an MPN coating, improved LN drainage and adjuvanticity of the particles in vivo. To examine whether any pathological side effects were caused by the Nanoadjuvant, major organs of mice were isolated and subjected to hematoxylin–eosin staining on day 7 post-injection (Figure S14, Supporting Information). Histological analysis showed no significant tissue abnormality, cell damage, or inflammatory cell infiltration compared to the saline group, suggesting the highly biocompatible nature of the Nanoadjuvant.

2.6. Cellular and Humoral Immunity Evoked by Antigen-Containing Nanoadjuvant

Based on the LN accumulation and immune activation of the Nanoadjuvant (with an MPN coating), we constructed a vaccine formulation containing both antigen and adjuvant by combining the Nanoadjuvant with a model antigen, OVA, and examined the antigen-specific immune responses in vivo. OVA was postloaded on the surface of the Nanoadjuvant (obtained after cargo loading and MPN coating), leading to a slight increase in diameter from 278 to 290 nm owing to protein adsorption (Figure S15a,b, Supporting Information). We also compared this loading method with preloading, that is, loading OVA within ASNs before MPN coating (Figure S15c, Supporting Information). The loading efficiency using the preloading method was lower at nanoparticle/OVA mass ratios smaller than 50, possibly due to the competition between CpG, siSTAT3, and OVA for pore occupancy on ASNs. In contrast, postloading facilitated loading of OVA at lower nanoparticle/OVA ratios, indicating that the MPN layer provides effective noncovalent interaction sites for OVA adsorption. The release profiles of CpG and siSTAT3 from the OVA-coated Nanoadjuvant (i.e., Nanoadjuvant-OVA) were assessed—OVA coating did not significantly influence the release of nucleic acids in serum-containing culture media (Figure S15d, Supporting Information). It is also worth noting that the postloading method led to greater LN deposition of OVA-Cy5 in mice after incorporation with an MPN layer (**Figure 5a**).

Subcutaneous administration (tail base) of the Nanoadjuvant-OVA vaccine was performed in C57BL/6 mice on day 0 and a booster on day 14 (Figure 5b). One week after the booster shot, spleen, and blood samples were collected from the

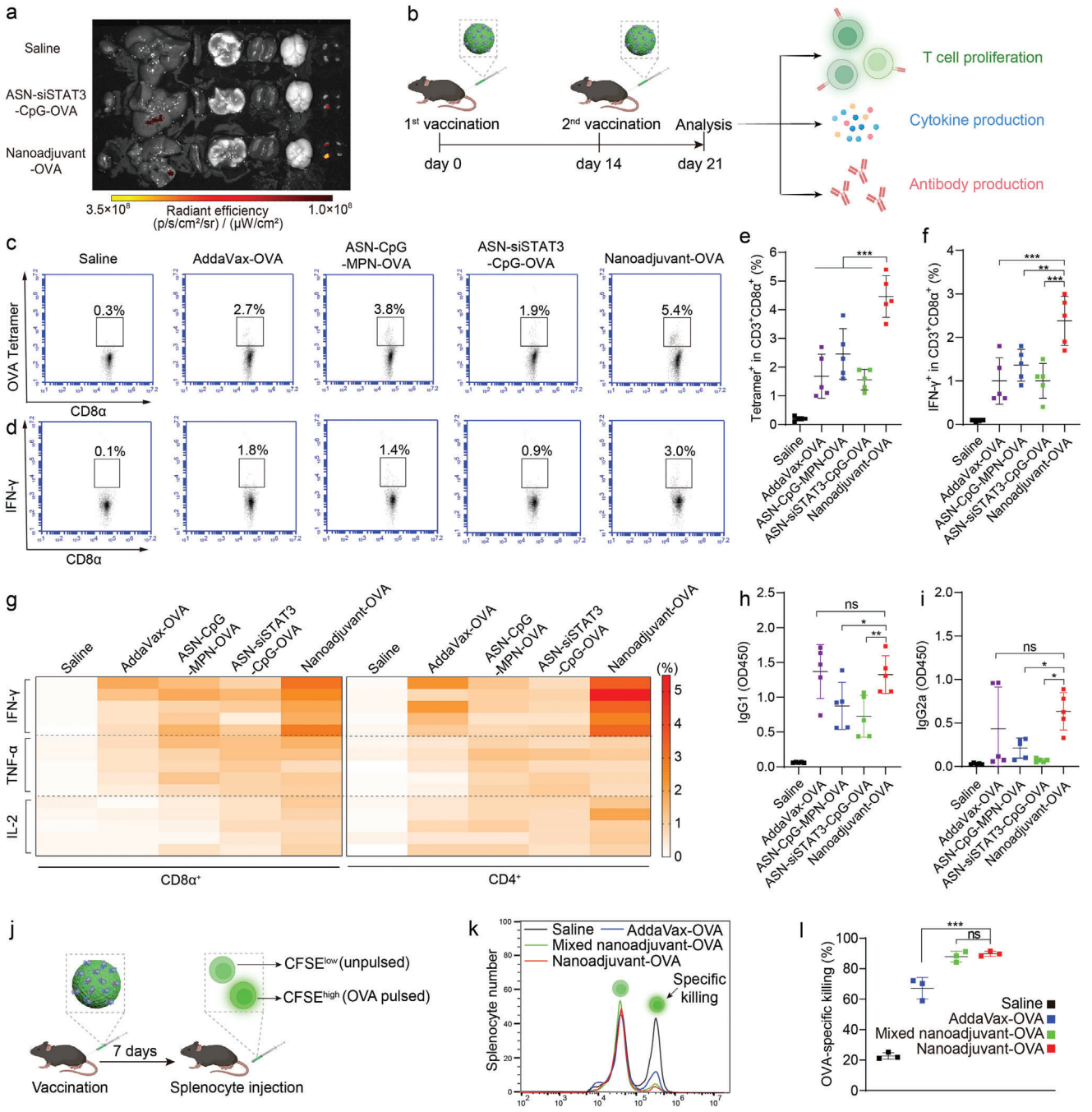

Figure 5. In vivo induction of OVA antigen-specific immune responses. a) Fluorescence images showing biodistribution of ASN-siSTAT3-CpG-OVA (without an MPN coating) and the Nanoadjuvant-OVA (with an MPN coating) among LNs and major organs harvested from C57BL/6 mice 24 h after subcutaneous tail base injections. OVA was labeled with Cy5. b) Schematic illustration of the two-dose vaccination study and subsequent analysis of immune responses, including T cell proliferation, cytokine production, and antibody production. Scatter plots and corresponding quantification of the frequency of c,e) OVA tetramer$^+$ CD8$^+$ and d,f) IFN-γ^+ CD8$^+$ T cells within splenocytes collected from vaccinated mice on day 21. Mice were divided into five vaccination groups: Saline, AddaVax-OVA (commercial adjuvant AddaVax with OVA), ASN-CpG-MPN-OVA (without siSTAT3), ASN-siSTAT3-CpG-OVA (without an MPN coating), and the Nanoadjuvant-OVA. g) Heat map showing the intracellular IFN-γ, TNF-α, and IL-2 production in spleen-derived CD8$^+$ T and CD4$^+$ T cells ($n = 5$ for each vaccination group). h,i) ELISA analysis of the production of anti-OVA IgG1 and IgG2a in mouse plasma collected on day 21. Data represent mean ± s.d. ($n = 5$). j) Schematic illustration of the CFSE-based antigen-specific cytotoxicity assay. k) Flow cytometry histogram and l) quantification analysis of OVA-specific CTL responses against injected splenocytes in vaccinated mice treated with saline, AddaVax-OVA, mixed nanoadjuvant-OVA (ASN-siSTAT3-MPN-OVA+ASN-CpG-MPN-OVA), or Nanoadjuvant-OVA. Data represent mean ± s.d. ($n = 3$). Statistical analysis was performed via one-way ANOVA with Tukey's multiple comparison test. $^*p < 0.05$, $^{**}p < 0.01$, $^{***}p < 0.001$, ns denotes nonsignificant.

immunized mice for T-cell and antibody analysis. The proliferation of antigen-specific T cells and the generation of antibodies reflect the level of cellular and humoral immune responses against diseases. Splenocytes and peripheral blood mononuclear cells were first examined using a H-2Kb-$OVA_{257-264}$ (SIINFEKL) tetramer to select for OVA-specific T cells. The frequency of tetramer$^+$ CD8$^+$ T cells in the Nanoadjuvant-OVA group was highest, indicating that the effective activation of APCs by nanoadjuvants led to a superior CTL response against OVA (Figure 5c–e; Figure S16, Supporting Information). In the absence of siSTAT3 or an MPN coating, the percentage of T cells responding to OVA presentation (i.e., vaccine efficacy) decreased, owing to the lack of an immunosuppression regulator and protective MPN layer. Furthermore, the Nanoadjuvant-OVA outperformed OVA emulsified in MF59 (AddaVax), a squalene-based oil-in-water commercial adjuvant. Therefore, the combination of the protective MPN layer and functional siSTAT3 contributed to superior OVA-specific T-cell responses displayed in vivo by the Nanoadjuvant-OVA. The splenocytes harvested from the immunized mice were also restimulated with $OVA_{257-264}$ (SIINFEKL) and the production of effector cytokines (i.e., interferon-γ (IFN-γ), TNF-α, and IL-2) were determined as a measurement of T-cell-mediated responses induced by the nanoadjuvants. Splenocytes treated with the Nanoadjuvant-OVA showed the highest frequency of IFN-γ-producing CD8$^+$ T and CD4$^+$ T cells among the splenocytes treated with the different vaccination groups (Figure 5d–g; Figure S17, Supporting Information). Moreover, TNF-α and IL-2 expression in both types of T cells from the Nanoadjuvant-OVA-treated group was comparable, if not better, to the AddaVax control. These findings suggest that the MPN coating and siSTAT3 downregulation can act synergistically to trigger strong APC- and T lymphocyte-mediated cellular immunity. In addition, the higher proportions of OVA-specific CD8$^+$ T cells stimulated by the Nanoadjuvants-OVA compared to a strong nanoformulation such as AddaVax indicate a strong capacity to promote cross-presentation of antigens.

The presence of anti-OVA immunoglobulin G (IgG) after vaccination with OVA-containing formulations indicates CD4helper T cell (CD4$^+$ T cell, Th)-related immunity. We assessed the production of two isotypes of anti-OVA IgG in mouse plasma using enzyme-linked immunosorbent assay (ELISA). The Nanoadjuvant-OVA induced a comparable level of anti-OVA IgG1 to the AddaVax-OVA positive control, suggesting that they both stimulated high Th2 (humoral) immune responses (Figure 5h). As for the measured level of production of anti-OVA IgG2a, which indicates Th1 (cellular) immune responses, there was no significant statistical difference between the Nanoadjuvant-OVA and AddaVax-OVA (Figure 5i). AddaVax is an example of an MF59 adjuvant, which mainly elicits a Th2-biased immune response.[26] Therefore, comparable results with AddaVax suggest that the Nanoadjuvant-OVA can evoke both strong humoral and cellular (both CD8$^+$T and Th) immune responses in vivo.

To further demonstrate the preventive and therapeutic potency of the nanoadjuvant, we examined the antigen-specific cytotoxic activity of CTLs in vaccinated mice using a flow cytometry assay based on the cell stain carboxyfluorescein succinimidyl ester (CFSE) (Figure 5j). In this assay, vaccinated mice were subsequently exposed to a mixture of OVA-pulsed (stimulated) splenocytes (CFSE^{high}-stained) and unpulsed splenocytes (CFSE^{low}-stained), and the cytotoxicity in the corresponding splenocyte populations was measured. In effective vaccination, CTLs from vaccinated mice are programmed to destroy antigen-specific target cells. The flow cytometry results showed that the highest percentage (≈90%) of OVA-pulsed (CFSE^{high}) splenocytes cytotoxicity, characterized by a reduction in cell number, was obtained from mice vaccinated with Nanoadjuvant-OVA, whereas the unpulsed (CFSE^{low}) splenocytes were unaffected (Figure 5k,l). This OVA-specific killing efficacy was comparable to that displayed by the mixed nanoadjuvant-OVA group (i.e., ASN-siSTAT3-MPN-OVA+ASN-CpG-MPN-OVA), indicating that the immunogenic agents (i.e., siSTAT3 and CpG) of the nanoadjuvant are functional even when separated on two nanoparticles. The antigen-specific killing efficacy of the nanoadjuvant could be supported by the proliferation of effector memory T cells triggered after vaccination (phenotypically characterized as CD44$^+$CD62L$^-$), which was highest with Nanoadjuvant-OVA (Figure S18, Supporting Information). This suggests that vaccination with Nanoadjuvant-OVA could promote downstream cellular and humoral immune responses upon re-exposure to the antigen. Simply changing the antigen in the nanoadjuvant could lead to specific reactivity toward other pathogens of infectious diseases or malignant tumor cells.

Throughout the vaccination period, no loss of body weight was observed across the mice cohorts (Figure S19, Supporting Information), confirming the high biocompatibility of our vaccine components. The biodegradability of the nanoadjuvants in vivo was assessed by scanning electron microscopy (SEM). Inguinal LNs from mice were harvested on days 2, 7, and 21 post injection, then fixed, dehydrated, and sectioned for SEM characterization (Figure S20, Supporting Information). The Nanoadjuvant-OVA appeared trapped as clusters in LNs on day 2 with observable spherical particle structures. Progressive degradation of the particles was evident at days 7 and 21. Our finding agrees with literature studies that demonstrate that silica-based nanoparticles with larger pore sizes have fast degradation rates,[27] potentially alleviating long-term accumulation in vivo.

3. Conclusion

We developed an MPN-based nanoadjuvant that effectively modulated immune responses both in vitro and in vivo. The nanoadjuvant was constructed using the innately immunoresponsive ASNs that encapsulated CpG, a strong adjuvant, and anti-STAT3 siRNA to silence an immunosuppression pathway and improve adjuvanticity. The MPN coating, which was applied following ASN synthesis and cargo loading, ensured the stability of the small nucleic acids during delivery, leading to enhanced LN accumulation and immune reactions. Histological examination of major mice organs revealed no apparent changes in cell and tissue morphology following administration of the nanoadjuvant, although detailed toxicity studies are warranted for future studies. Further formulation of the nanoadjuvant with the model antigen OVA triggered strong cellular and humoral immunity in mice compared with controls. It is noted that the preparation of nanoadjuvant and the nanoadjuvant-based vaccine is simply based on layer-by-layer deposition on ASN templates that facilitates high cargo loading capacity. The high biocompatibility of the

ASN-MPN platform opens avenues for expanding its application in biomedicine, including cancer immunotherapy. For instance, personalized cancer vaccines can be constructed based on this platform by replacing OVA with other specific neoantigens. The porosity of the ASN combined with the interactive nature of the MPN could facilitate the loading of various biomolecules for a multifunctional vaccine platform. The modularity of MPN assembly affords a diverse choice of polyphenol and metal ion building blocks that can be used for further nanoparticle engineering to improve cargo loading and APC interactions, and boost immune responses. Considering the limited immunological research involving MPN-based materials, our findings provide insights and showcase the potential to propel the advancement of constructing metal–organic-based adjuvants and vaccines.

Supporting Information

Supporting Information is available from the Wiley Online Library or from the author.

Acknowledgements

This work received financial support from the Australian National Health and Medical Research Council under the Program Grant scheme (F.C., GNT1149990) and the Innovation Project of Jinan Science and Technology Bureau (J.C., 2020GXRC022). This work was performed in part at the Materials Characterization and Fabrication Platform (MCFP) at The University of Melbourne and the Victorian Node of the Australian National Fabrication Facility (ANFF), Peter Doherty Institute, and Ian Holmes Imaging Centre at Bio21. Figures were partly created using BioRender. The authors thank Prof. Hans Acha-Orbea (University of Lausanne) for gifting the DC1940 cell line, and Prof. Andrew Brooks (Peter Doherty Institute for Infection and Immunity) for preparation and donation of H-2Kb-SIINFEKL tetramer. The authors thank Dr. Wanjun Xu (The University of Melbourne) for the helpful discussions.

Open access publishing facilitated by The University of Melbourne, as part of the Wiley - The University of Melbourne agreement via the Council of Australian University Librarians.

Conflict of Interest

The authors declare no conflict of interest.

Data Availability Statement

The data that support the findings of this study are available from the corresponding author upon reasonable request.

Keywords

immunosuppressive pathways, metal–phenolic networks, nanoadjuvants, RNA interference

Received: March 25, 2024
Revised: May 19, 2024
Published online:

[1] S. G. Reed, M. T. Orr, C. B. Fox, *Nat. Med.* **2013**, *19*, 1597.
[2] a) I. Mellman, G. Coukos, G. Dranoff, *Nature* **2011**, *480*, 480; b) J. Tan, B. Ding, B. Teng, P. a. Ma, J. Lin, *Adv. Funct. Mater.* **2022**, *32*, 2111670.
[3] D. M. Klinman, *Nat. Rev. Immunol.* **2004**, *4*, 249.
[4] a) P. Marrack, A. S. McKee, M. W. Munks, *Nat. Rev. Immunol.* **2009**, *9*, 287; b) B. Sun, Z. Ji, Y.-P. Liao, M. Wang, X. Wang, J. Dong, C. H. Chang, R. Li, H. Zhang, A. E. Nel, T. Xia, *ACS Nano* **2013**, *7*, 10834; c) P. J. Hotez, D. B. Corry, U. Strych, M. E. Bottazzi, *Nat. Rev. Immunol.* **2020**, *20*, 399.
[5] G. N. Barber, *Nat. Rev. Immunol.* **2015**, *15*, 760.
[6] G. Dranoff, *Nat. Rev. Cancer* **2004**, *4*, 11.
[7] a) D. J. Irvine, M. C. Hanson, K. Rakhra, T. Tokatlian, *Chem. Rev.* **2015**, *115*, 11109; b) G. Zhu, F. Zhang, Q. Ni, G. Niu, X. Chen, *ACS Nano* **2017**, *11*, 2387; c) X. Li, X. Wang, A. Ito, *Chem. Soc. Rev.* **2018**, *47*, 4954; d) F. J. Zhu, Y. L. Tong, Z. Y. Sheng, Y. M. Yao, *Acta Biomater.* **2019**, *94*, 132; e) H. Dong, Q. Li, Y. Zhang, M. Ding, Z. Teng, Y. Mou, *Adv. Sci.* **2023**, *10*, 2301339; f) N. Wang, G. Zhang, P. Zhang, K. Zhao, Y. Tian, J. Cui, *Adv. Healthcare Mater.* **2023**, *12*, 2300249.
[8] a) J. Xu, J. Lv, Q. Zhuang, Z. Yang, Z. Cao, L. Xu, P. Pei, C. Wang, H. Wu, Z. Dong, Y. Chao, C. Wang, K. Yang, R. Peng, Y. Cheng, Z. Liu, *Nat. Nanotechnol.* **2020**, *15*, 1043; b) J. Liu, H. J. Li, Y. L. Luo, Y. F. Chen, Y. N. Fan, J. Z. Du, J. Wang, *Nano Lett.* **2020**, *20*, 4882.
[9] a) D. N. Nguyen, K. P. Mahon, G. Chikh, P. Kim, H. Chung, A. P. Vicari, K. T. Love, M. Goldberg, S. Chen, A. M. Krieg, J. Chen, R. Langer, D. G. Anderson, *Proc. Natl. Acad. Sci. U.S.A.* **2012**, *109*, E797; b) H. Liu, K. D. Moynihan, Y. Zheng, G. L. Szeto, A. V. Li, B. Huang, D. S. Van Egeren, C. Park, D. J. Irvine, *Nature* **2014**, *507*, 519.
[10] a) X. Hou, T. Zaks, R. Langer, Y. Dong, *Nat. Rev. Mater.* **2021**, *6*, 1078; b) M. J. Mitchell, M. M. Billingsley, R. M. Haley, M. E. Wechsler, N. A. Peppas, R. Langer, *Nat. Rev. Drug Discov.* **2021**, *20*, 101.
[11] a) M. Saeed, F. Chen, J. Ye, Y. Shi, T. Lammers, B. G. De Geest, Z. P. Xu, H. Yu, *Adv. Mater.* **2021**, *33*, 2008094; b) D. Lee, K. Huntoon, Y. Wang, W. Jiang, B. Y. S. Kim, *Adv. Mater.* **2021**, *33*, 2007576.
[12] a) M. Kortylewski, P. Swiderski, A. Herrmann, L. Wang, C. Kowolik, M. Kujawski, H. Lee, A. Scuto, Y. Liu, C. Yang, J. Deng, H. S. Soifer, A. Raubitschek, S. Forman, J. J. Rossi, D. M. Pardoll, R. Jove, H. Yu, *Nat. Biotechnol.* **2009**, *27*, 925; b) J. H. Kim, Y.-W. Noh, M. B. Heo, M. Y. Cho, Y. T. Lim, *Angew. Chem., Int. Ed.* **2012**, *124*, 9808; c) H. Yu, H. Lee, A. Herrmann, R. Buettner, R. Jove, *Nat. Rev. Cancer* **2014**, *14*, 736; d) G. Zhu, L. Mei, H. D. Vishwasrao, O. Jacobson, Z. Wang, Y. Liu, B. C. Yung, X. Fu, A. Jin, G. Niu, Q. Wang, F. Zhang, H. Shroff, X. Chen, *Nat. Commun.* **2017**, *8*, 1482.
[13] R. L. Setten, J. J. Rossi, S.-p. Han, *Nat. Rev. Drug Discov.* **2019**, *18*, 421.
[14] a) Y. Chen, H. Chen, J. Shi, *Adv. Mater.* **2013**, *25*, 3144; b) S. Dong, Z. Feng, R. Ma, T. Zhang, J. Jiang, Y. Li, Y. Zhang, S. Li, X. Liu, X. Liu, H. Meng, *Nano Lett.* **2023**, *23*, 2137; c) J. Tan, B. Ding, H. Chen, Q. Meng, J. Li, C. Yang, W. Zhang, X. Li, D. Han, P. Zheng, P. Ma, J. Lin, *Small* **2023**, *20*, 2305567.
[15] Y. Yang, J. Tang, H. Song, Y. Yang, Z. Gu, J. Fu, Y. Liu, M. Zhang, Z.-A. Qiao, C. Yu, *Angew. Chem., Int. Ed.* **2020**, *59*, 19610.
[16] H. Ejima, J. J. Richardson, K. Liang, J. P. Best, M. P. v. Koeverden, G. K. Such, J. Cui, F. Caruso, *Science* **2013**, *341*, 154.
[17] H. Geng, Q.-Z. Zhong, J. Li, Z. Lin, J. Cui, F. Caruso, J. Hao, *Chem. Rev.* **2022**, *122*, 11432.
[18] a) J. Guo, Y. Ping, H. Ejima, K. Alt, M. Meissner, J. J. Richardson, Y. Yan, K. Peter, D. von Elverfeldt, C. E. Hagemeyer, F. Caruso, *Angew. Chem., Int. Ed.* **2014**, *53*, 5546; b) Z. Lin, J. Zhou, Y. Qu, S. Pan, Y. Han, R. P. M. Lafleur, J. Chen, C. Cortez-Jugo, J. J. Richardson, F. Caruso, *Angew. Chem., Int. Ed.* **2021**, *60*, 24968.
[19] a) M. Shin, J. H. Ryu, J. P. Park, K. Kim, J. W. Yang, H. Lee, *Adv. Funct. Mater.* **2015**, *25*, 1270; b) J. X. Fan, D. W. Zheng, W. W. Mei, S. Chen, S. Y. Chen, S. X. Cheng, X. Z. Zhang, *Small* **2017**, *13*, 1702714; c) Z. Zhang, W. Sang, L. Xie, W. Li, B. Li, J. Li, H. Tian, Z. Yuan, Q. Zhao, Y. Dai, *Angew. Chem., Int. Ed.* **2021**, *60*, 1967; d) J. Chen, S. Pan, J. Zhou,

Z. Lin, Y. Qu, A. Glab, Y. Han, J. J. Richardson, F. Caruso, *Adv. Mater.* **2022**, *34*, 2108624; e) Q. Fan, Z. Yang, Y. Li, Y. Cheng, Y. Li, *Adv. Funct. Mater.* **2021**, *31*, 2101046.

[20] J. Chen, S. Pan, J. Zhou, R. Seidel, S. Beyer, Z. Lin, J. J. Richardson, F. Caruso, *Chem. Mater.* **2021**, *33*, 2557.

[21] M. Faria, M. Bjornmalm, K. J. Thurecht, S. J. Kent, R. G. Parton, M. Kavallaris, A. P. R. Johnston, J. J. Gooding, S. R. Corrie, B. J. Boyd, P. Thordarson, A. K. Whittaker, M. M. Stevens, C. A. Prestidge, C. J. H. Porter, W. J. Parak, T. P. Davis, E. J. Crampin, F. Caruso, *Nat. Nanotechnol.* **2018**, *13*, 777.

[22] a) G. Yun, J. J. Richardson, M. Capelli, Y. Hu, Q. A. Besford, A. C. G. Weiss, H. Lee, I. S. Choi, B. C. Gibson, P. Reineck, F. Caruso, *Adv. Funct. Mater.* **2019**, *30*, 1905805; b) J. Chen, S. Pan, J. Zhou, Z. Lin, Y. Qu, A. Glab, Y. Han, J. J. Richardson, F. Caruso, *Adv. Mater.* **2022**, *34*, 2108624.

[23] a) Y. Ju, J. Cui, M. Mullner, T. Suma, M. Hu, F. Caruso, *Biomacromolecules* **2015**, *16*, 807; b) X. He, G. Gong, M. Chen, H. Zhang, Y. Zhang, J. J. Richardson, W. Y. Chan, Y. He, J. Guo, *Angew. Chem., Int. Ed.* **2024**, *63*, 202314501.

[24] J. Tschopp, K. Schroder, *Nat. Rev. Immunol.* **2010**, *10*, 210.

[25] a) S. T. Reddy, A. Rehor, H. G. Schmoekel, J. A. Hubbell, M. A. Swartz, *J. Controlled Release* **2006**, *112*, 26; b) V. Manolova, A. Flace, M. Bauer, K. Schwarz, P. Saudan, M. F. Bachmann, *Eur. J. Immunol.* **2008**, *38*, 1404; c) J. A. Hubbell, S. N. Thomas, M. A. Swartz, *Nature* **2009**, *462*, 449.

[26] B. Guy, *Nat. Rev. Microbiol.* **2007**, *5*, 396.

[27] a) D. Shen, J. Yang, X. Li, L. Zhou, R. Zhang, W. Li, L. Chen, R. Wang, F. Zhang, D. Zhao, *Nano Lett.* **2014**, *14*, 923; b) X. Hong, X. Zhong, G. Du, Y. Hou, Y. Zhang, Z. Zhang, T. Gong, L. Zhang, X. Sun, *Sci. Adv.* **2020**, *6*, eaaz4462.